Dielectron satellites of resonance lines of Ne-like ions in high-temperature plasmas

S. Ya. Khakhalin, B. A. Bryunetkin, I. Yu. Skobelev, A. Ya. Faenov

Scientific-Industrial Union "Russian Research Institute for Physicotechnical and Radio Engineering Measurements," 141570 Mendeleevo, Moscow District, Russia

J. Nilsen and A. L. Osterheld

Livermore National Laboratory, California, USA

S. A. Pikuz

P.N. Lebedev Physical Institute of Russian Academy of Sciences, 117924 Moscow, Russia

We analyze experimentally and theoretically the spectrum of dielectron satellites of resonance lines of neon-like ions. Spectra of lines due to stabilizing radiative transitions from doubly excited states of Ne-like Y, Zr, Nb, and Mo ions are recorded with high spectral resolution, $\lambda/\Delta\lambda \sim 500$. Spectra of yttrium, zirconium, niobium, and molybdenum ions are obtained using laser plasmas. Satellite lines or compact groups of lines belonging to Y XXIX, Zr XXX, Nb XXXI, and Mo XXXII ions are identified for the first time, and their wavelengths are measured with a precision to ± 2 mÅ. Good correspondence of the model and the experimental spectra demonstrates the great promise of using line radiation of Na-like ions for high-temperature plasma diagnostics.

1. INTRODUCTION

A typical feature of plasma x-ray spectra is the presence of lines corresponding to transitions from doubly-excited energy levels of multiply charged ions present in plasmas. These lines, called dielectron satellites, are observed in the spectra of laboratory sources and astrophysical objects.

The most easily accessible to observation and analysis are satellites of resonance lines of K-ions (ions for which the K-shell is the basic one) resulting from transitions in two-and three-electron ions. They are well-studied and widely used for plasma diagnostics. The relative simplicity of these satellites allows for reliable calculation of spectral transition wavelengths and radiative–collisional characteristics. For example, the accuracy $\Delta\lambda$ of theoretical calculations of the wavelengths λ is $\Delta\lambda/\lambda \sim 10^{-4}$ for these lines, which is comparable to the measurement accuracy. For this reason, experimental spectra of K-ions are usually explained exhaustively on the basis of existing theoretical models, and serve as a rich source of information on plasma physical parameters.[1]

The interpretation of spectra containing satellite lines resulting from transitions in ions with more than three electrons, i.e., in Be-, B-, C-, N-, O-, and F-like ions, is a much more complicated problem, as is the identification of dielectron satellites of resonance lines of L-ions, among which satellite structures near resonance lines of Ne-like ions are of special interest. This is associated with the following factors:

First, Ne-like ions require the least energy for formation among all L-ions, i.e., ions whose basic shell configuration is $1s^2 2s^k 2p^l$ ($k = 1,2$; $l = 1,2,...,6$).

Second, due to the closed basic shell, in which the only level is $^1S_0$ due to the basic configuration $1s^2 2s^2 2p^8$, the

short-wavelength spectrum of Ne-like ion radiation has a simple form, reducing in essence to seven Rydberg series of dipole transitions of the type $(2s^2 2p^6 - 2s^2 2p^5 ns, nd)$ and $(2s^2 2p^6 - 2s 2p^6 np)$. These seven series can be reliably detected, together with their satellites, in the x-ray spectra of hot plasmas, and can be followed rather far along the isoelectronic sequence.

The third factor, which particularly increased interest in the satellite structure of resonance lines of Ne-like ions, is related to progress in producing short-wavelength lasers for 3–3 transitions of these ions,[2] as well as recent proposals concerning utilization of Ne-like ions in laser systems with photopumping.[3,4] The magnitude of the inverted population formed in such lasers depends heavily on plasma density and temperature, as well as on the concentration of Ne- and Na-like ions present in it (see, for instance, Ref. 5). The need to optimize active medium parameters with the aim of producing maximum possible gain coefficients naturally leads to attempts to use the information capacity of satellite structures accompanying the lines of Ne-like ions for plasma diagnostics.

Attempts to interpret dielectron satellites of resonance lines of Ne-like ions and to use them for plasma parameter diagnostics were made in Refs. 6–12. However, insufficient spectral resolution in these experiments and the lack of accurate theoretical data precluded any significant advance to be made in investigating satellites of this type. In our previous work,[13–15] spectra of Na-like satellites of copper, zinc, and selenium ions were first recorded and identified with high spectral resolution. The interpretation of that spectrum, which was successful on the whole, showed however that the comparatively light ions indicated are not optimal for a general estimate of the quality of theoretical calculations, because a considerable number of intense

2s2p^6

2s^{2}2p^5

3d
3p

2s2p^6
3s

dielectron capture

$$2s^2 2p^6 + e^- \longrightarrow \begin{Bmatrix} 2s2p^6\, 3l3l' \\ 2s^2 2p^5\, 3l3l' \end{Bmatrix}$$

3d

3p
3d

2s^{2}2p^5
3s

Ne

3p^2 3s3d 3p3d 3d^2

2s2p^6

3s^2 3s3p 3p^2 3s3d 3p3d 3d^2

3s^2 3s3p

2s^{2}2p^5

2s^{2}2p^6

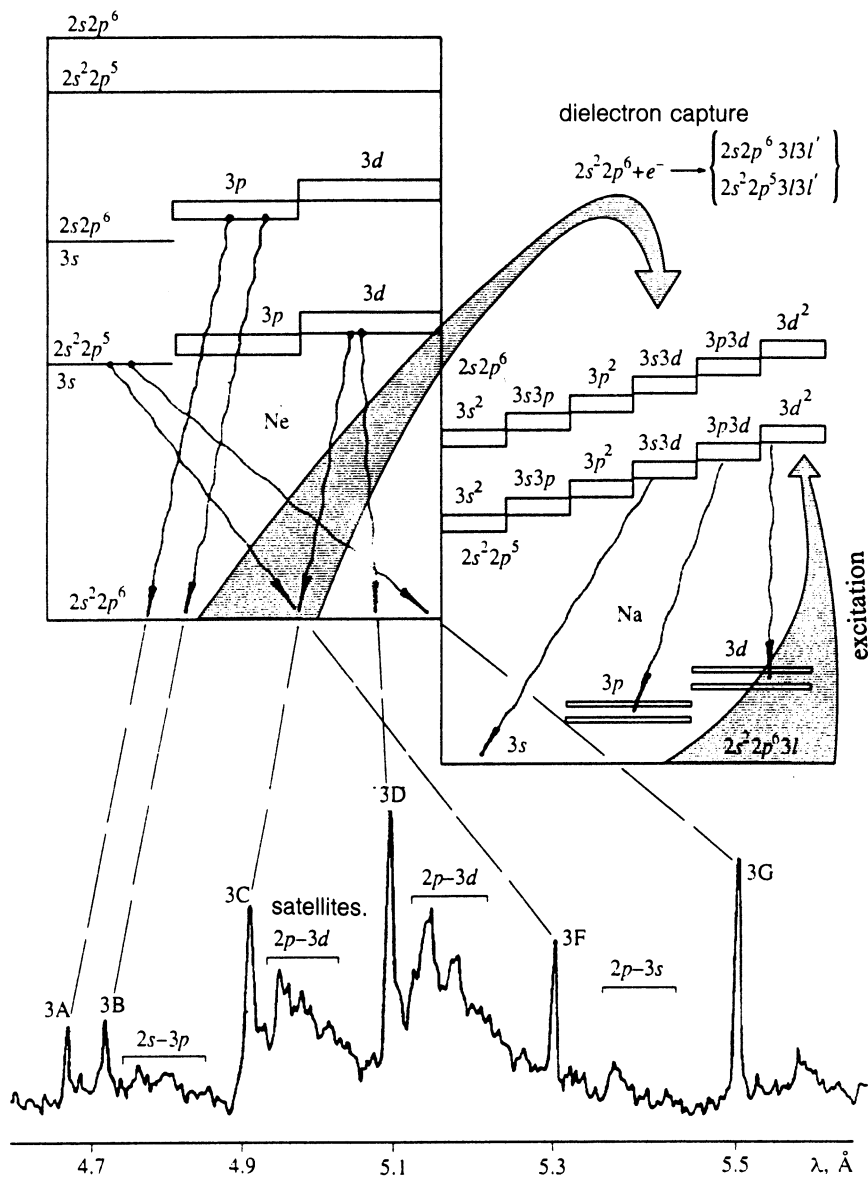Na

excitation

3d

3p

3s

2s^{2}2p^{6}3l

FIG. 1. Energy level diagram of Ne-like and Na-like ions. Two mechanisms of populating autoionization states are shown. A portion of the niobium x-ray spectrum is presented containing resonance lines of the Ne-like ion 2s–3p (3A,3B), 2p–3d (3C,3D), 2p–3s (3F,3G) together with the corresponding satellites.

3D

3C satellites.
2p–3d

2p–3d

2p–3s

3F

3G

3A 3B

2s–3p

4.7   4.9   5.1   5.3   5.5   λ, Å

lines belonging to ions of higher multiplicities (F- and O-like) are superimposed on the satellite spectrum in these cases.

In the present work, spectra of elements heavier than in Refs. 13–15 (yttrium, zirconium, niobium, and molybdenum) are studied. The transition to heavier elements made it possible to shift the ionization equilibrium toward ions of lower multiplicity and to obtain spectra free of lines from ions of higher multiplicities. As a result of this work, calculations of the satellite line constants were performed for a number of elements for the first time, and satellite line wavelengths were measured to high accuracy. This enables the quality of theoretical calculations of multiply charged multielectron ion structure to be assessed.

2. RECORDING AND CALCULATIONS OF THE SPECTRA

Spectra were obtained in the experiments with laser-produced plasmas.[6,7] A neodymium laser with an output energy of up to 80 J and pulse length of ~2 ns provided a power flux density of ~5 · 10^{14} W/cm^2 on a target. The

spectra were recorded with a defocusing spectrograph with a convex mica crystal,[6] with a spectral resolution $\lambda/\Delta\lambda \geqslant 500$ in the third reflection order. In measuring the wavelengths, the spectral lines of Ne-like ions were used as references for constructing the spectrograph dispersion curve. The error in measuring the wavelengths of individual lines was determined mainly by the error in the reference wavelengths, and did not exceed ±2 mÅ. When the peak observed on film was a combination of several unresolved spectral transitions, the measurement accuracy was naturally lower, and was determined by the spectral width of the peak. The spectral lines of Y XXIX, Zr XXX, Nb XXXI, and Mo XXXII ions were identified by comparing the wavelengths and intensities of the observed lines with theoretical calculations. The Dirac–Fock multiconfigurational approximation was used to calculate the energy structure and the probabilities of radiative and autoionization processes. The calculation technique is presented in Ref. 16. All $2l3l3l' \rightarrow 3l''$ dipole transitions were taken into consideration ($2l$ denotes a hole in the neon-like shell,
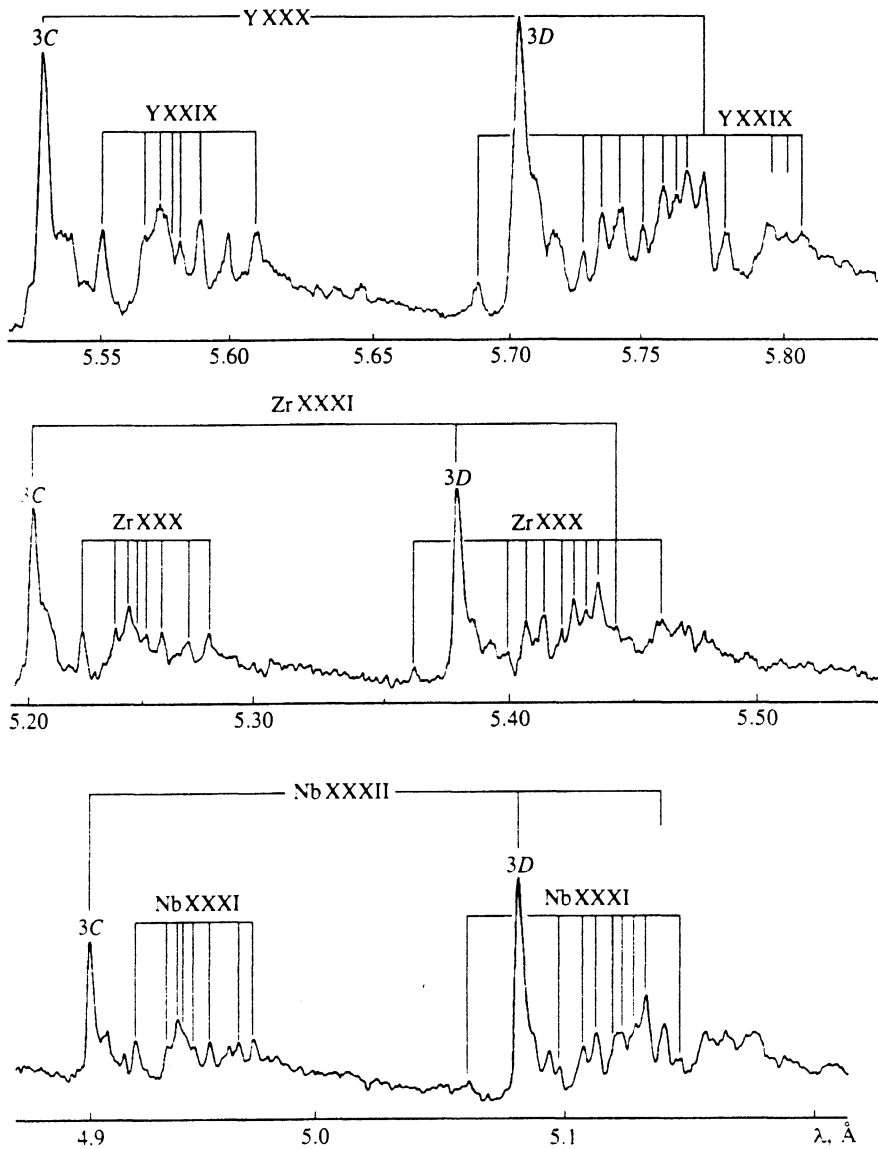
FIG. 2. Densitograms of x-ray spectra of Ne-like ions near the $2p$–$3d$ (3C,3D) resonance lines. Denoted are dielectron satellites resulting from transitions in Na-like ions.

$3l3l'$ denotes two electrons with $n=3$). The $\overline{2l3l3l'}$ shell consists of 237 doubly excited states, which are coupled to the $1s^2 2s^2 2p^6$ ground state of a neon-like ion via Auger transitions, and to the five $[KL]3s_{1/2},3p_{1/2},3p_{3/2}$ nonautoionization states via radiative transitions. [KL] denotes filled K- and L-shells.

3. GENERAL DESCRIPTION OF THE SPECTRUM

X-ray spectra analyzed in this work can be presented in the generalized form given in Fig. 1 together with energy level diagrams of Ne- and Na-like ions. Transitions to the $2s^2 2p^6 \, ^1S_0$ ground state of a Ne-like ion form seven intense series whose head lines corresponding to transitions from states with $n=3$ are given in the figure: 3A ($^1S_0$–$2s2p^6 3p \, ^1P_1$), 3B ($^1S_0$–$2s2p^6 3p \, ^3P_1$), 3C ($^1S_0$–$2s^2 2p^5 3d \, ^1P_1$), 3D ($^1S_0$–$2s^2 2p^5 3d \, ^3D_1$), 3E ($^1S_0$–$2s2p^6 3d \, ^3P_1$), 3F ($^1S_0$–$2s^2 2p^5 3s \, ^3P_1$), and 3G ($^1S_0$–$2s^2 2p^5 3s \, ^1P_1$). Less intense lines of a Ne-like ion, for instance, magnetic quadrupole transitions ($^1S_0$–$2s^2 2p^5 ns \, ^3P_2$), are not shown in the figure. The line 3E is blended with intense p–d satellites

belonging to a Na-like ion, and as will be shown below, earlier measurements of the wavelength of the 3E line are largely doubtful. For the purposes of the present work, it is important that a group of resonance lines of a Ne-like ion is distributed over the whole spectral range considered, allowing for the reliable interpolation of wavelengths. For the reason given above, the 3E line was not used as a reference.

The spectrum of a F-like ion has a significantly more complicated structure: 34 allowed electric dipole transitions of the $2p^5$–$2p^4 3d$ type mainly between the lines 3B and 3C, and 14 transitions of the $2p^5$–$2p^4 3s$ type between the lines 3D and 3F. The shortest-wavelength $2p^5$–$2p^4 3d$ lines partially overlap long-wavelength lines of the $2p^4$–$2p^3 3d$ spectral group of an O-like ion. $2s$–$3p$ transitions of an F-like ion also lie in the same range. Another group of lines of O-like ions corresponding to $2p^4$–$2p^3 3p$ transitions lies in the vicinity of the 3C and 3D lines, which overlap most strongly with $2p$–$3d$ transitions of the Na-like satellites studied in this work. It is important to note that experimental spectra (see Fig. 2) are indicative of a con-
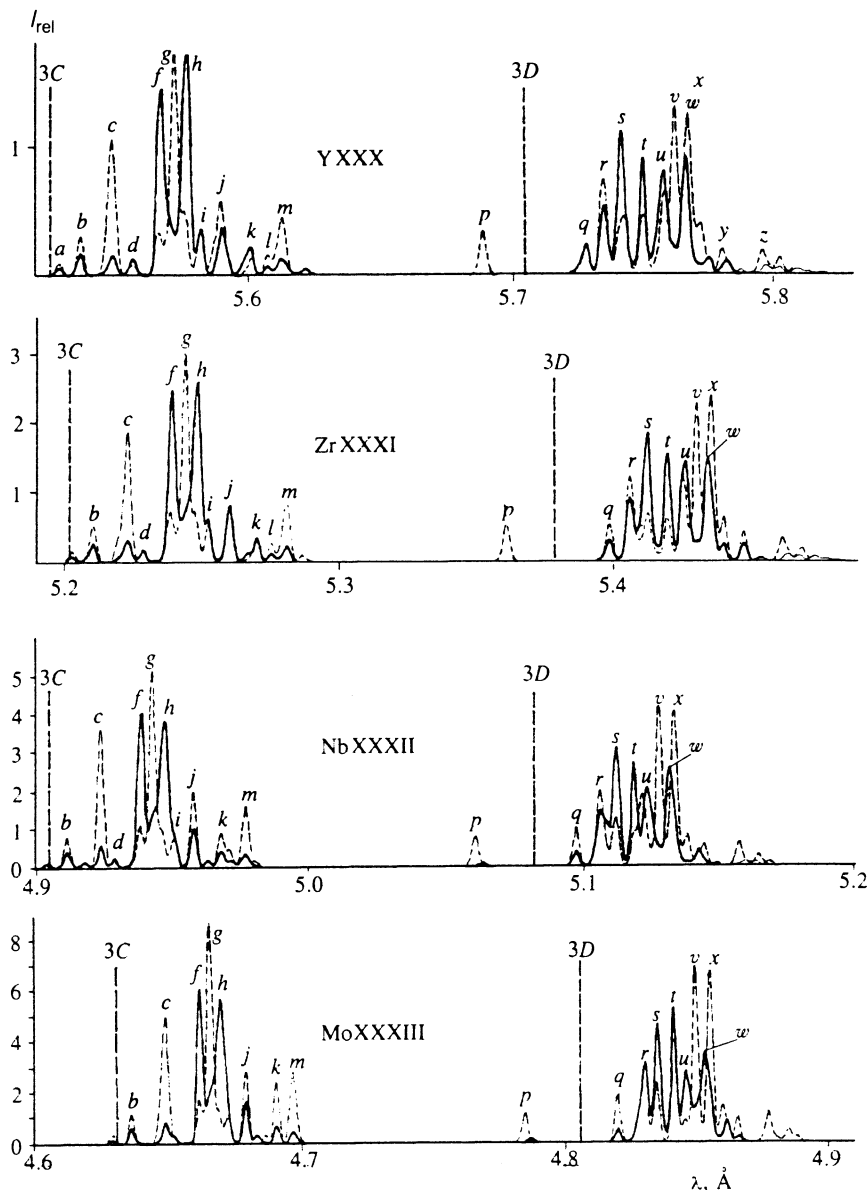
FIG. 3. Calculated spectra of dielectron satellites of $2p-3d$ resonance lines of neon-like ions of yttrium, zirconium, niobium, and molybdenum. Spectra formed when autoionization states of Na-like ion are populated only by dielectron capture and by inner-shell excitation via electron impact are shown by the dashed lines and the solid lines, respectively. The positions of the resonance lines of Ne-like ions are shown by vertical dashes.

siderable decrease in the relative intensities of lines of F-like and O-like ions as compared to the spectra of lighter elements (see Refs. 13–15) recorded with the same laser pulse parameters.

4. CONSTRUCTION OF A MODEL SPECTRUM. COMPARISON WITH EXPERIMENT

The electron density of laser-produced plasmas was in this work of order $N_e \sim 10^{20}-10^{21}$ cm^{-3}. On the one hand, the $2s^2 2p^6 3s$, $2s^2 2p^6 3p$, and $2s^2 2p^6 3d$ states of a Na-like ion are collisionally mixed at such densities. On the other, the kinetics of its doubly excited states corresponds to the coronal model, which makes it possible to include the population of autoionization levels due to only two types of processes: dielectron capture and direct excitation of $2s^2 2p^6 3l$ levels via electron impact:

$$2s^2 2p^6 + e^- \to (\overline{2l3l3l'})2s^2 2p^6 3l + e^- \to (\overline{2l3l3l'}) + e^-.$$
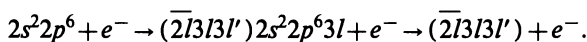
Under the conditions indicated, the intensity I_{ik} of the dielectron satellite corresponding to the transition from the

doubly excited level i (one of the 237 levels $2l3l'3l''$) to the level k (one of the five levels $2s^2 2p^6 3l$) can be represented as a sum of two terms,

$$I_{ik} = \hbar w_{ik} \left[\langle v\sigma \rangle^d \frac{A_{ik}}{\Gamma_i + \Sigma_j A_{ij}} N(\text{Ne}) N_e \right.$$
$$\left. + \langle v\sigma \rangle^{ex} \frac{A_{ik}}{\Gamma_i + \Sigma_j A_{ij}} N(\text{Na}) N_e \right], \tag{1}$$

where Γ_i, $\langle v\sigma \rangle^d$, and $\langle v\sigma \rangle^{ex}$ are the autoionization rate, the dielectron capture rate, and the electron impact excitation rate; $N(\text{Ne})$ and $N(\text{Na})$ are the concentrations of Ne- and Na-like ions, A_{ij} is the probability of radiative transition $i \to j$, and $\Sigma_j A_{ij} = A_i$ is the total probability of radiative decay from the state i.

Model spectra of Na-like ions Y XXIX, Zr XXX, Nb XXXI, and Mo XXXII in the vicinity of the 3C ($2p^6$ $^1S_0-2p^5 3d$ $^1P_1$), 3D ($2p^6$ $^1S_0-2p^5 3d$ $^3D_1$), and 3E ($2p^6$ $^1S_0-2p^5 3d$ $^3P_1$) resonance lines are presented in Fig. 3. The dashed lines show the spectra obtained in the limiting case
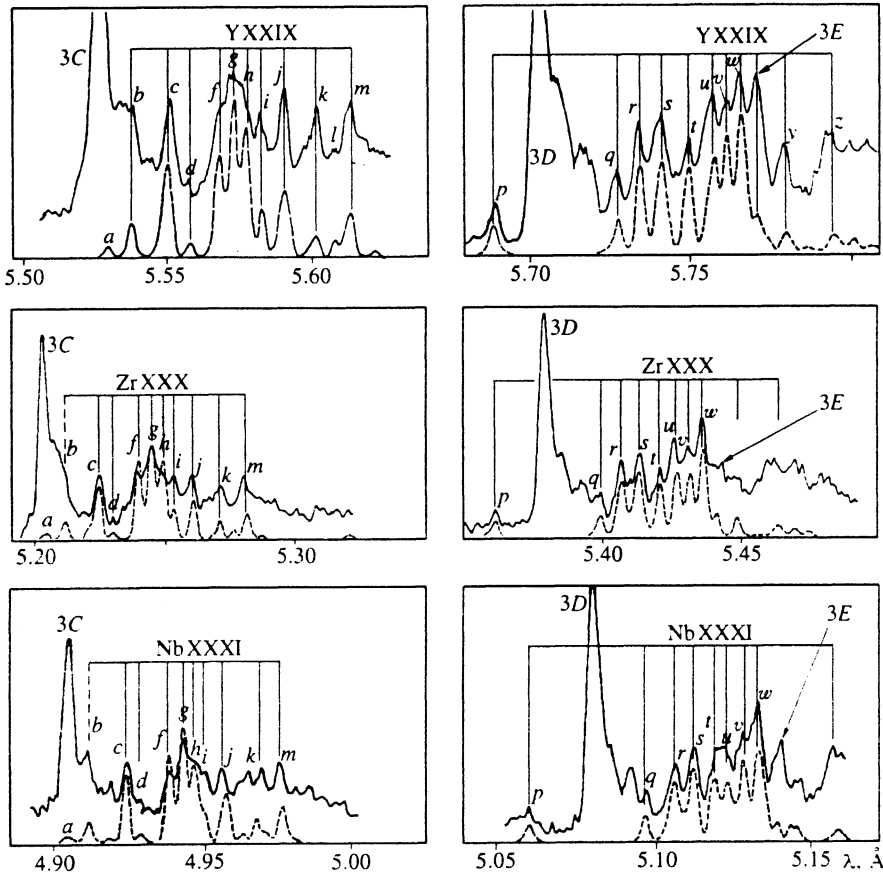
FIG. 4. Densitograms of portions of experimental spectra of Ne-like ions (solid curves) together with results of numerical simulation (dashed curves) of spectra of dielectron satellites. The labeling of the lines is explained in the table.

of autoionization level population only through dielectron capture. The spectrum presented by the solid curves corresponds to the opposite case, in which excitation of the inner shell of a Na-like ion via electron impact is the only channel of satellite excitation. In both cases, the spectral transition profiles were assumed Gaussian. The positions of the resonance lines of Ne-like ions are denoted by the vertical lines in Fig. 3.

It is seen from Fig. 3 that the satellite spectra of the four elements in question are highly similar, so it is possible to introduce common letter designators. These appear in Fig. 3, and they will be used below in the table of wavelengths. For each of the elements, the shapes of envelopes shown by solid and dashed lines in Fig. 3 are so different that even the number of peaks changes when passing from one regime to another. The peaks c, g, p, v, and x result mainly from dielectron capture, the peaks f, h, and w are mainly due to excitation from sodium-like ions. However, it is important to note that most of the peaks are combinations of several lines, and separating the peaks into "preferentially dielectron" and "excited by electron impact only" appears to be highly arbitrary.

In the simulation of experimental spectra, the electron temperature was arbitrarily fixed at $T_e = z^2$ [eV] (z is the spectroscopic symbol of an ion), and the concentration ratio of Ne- and Na-like ions was selected in each case to yield the best agreement between experimental and model spectra. This ratio was in the range $N(\text{Ne})/N(\text{Na}) = 1$–1.5 for all four elements.

The results of modeling the envelope of dielectron sat-

ellites are presented in Fig. 4 (dashed curves) along with the corresponding portions of the experimental spectra (solid curves). Comparison of the theoretical and the experimental envelopes shows that the correspondence between theory and experiment is mostly very good. The results of a comparison of the measured and the calculated wavelengths for the four elements are given in the table, together with the spectroscopic notation for the most intense components of each of the satellite peaks, and the calculated values of the probabilities of radiative decay and autoionization. The intensity factors Qd of transitions $i \rightarrow j$ included in the table are defined in the traditional way:

$$Qd(i \rightarrow f) = \frac{g_i A_{if} \Gamma_i}{A_i + \Gamma_i}, \tag{2}$$

where g_i is the statistical weight of the autoionization level. More complete information on all of the the satellite transitions included can be obtained from the tables of Ref. 16, where calculated results are available for yttrium and molybdenum ions.

Let us discuss in more detail the correlation between the wavelengths and the intensities of satellite peaks obtained theoretically and experimentally.

For all four elements, the a peak is inside the 3C line and contributes additionally to its intensity. The b peak corresponds to within 1 mÅ to our calculations in all four cases: $\lambda_{\text{theor}} - \lambda_{\text{exp}} \simeq 1$ mÅ. The visual intensity of the peak exceeds the calculated results several-fold, but the peak

itself is clearly located on a pedestal formed by the long-wavelength wing of the 3C line.

The peak c is most clearly separated from other lines, and its shape can be used to assess the validity of modeling the line-broadening magnitude. The discrepancy between the experimental and the theoretical wavelengths is less

TABLE I. Experimental and theoretical wavelengths, calculated radiative probabilities A, probabilities of dielectron capture Γ, and intensity factors Qd for satellites of resonance lines of Ne-like ions. *Note.* In labeling the upper autoionization level, the symbols a or b denote holes in the inner shell: $a=2s^2 2p_{1/2}^2 2p_{3/2}^3$, $b=2s^2 2p_{1/2} 2p_{3/2}^4$. Single-electron states of the outer shell represented in the form 3l* or 3l_ denote $j=l+1/2$ for 3l* and $l-1/2$ for 3l_, i.e., $s*=3s_{1/2}$, $3p=3p_{1/2}$, $3d=3d_{3/2}$, $3d*=3d_{5/2}$. [KL] denotes filled K and L shells. 1.35+14 denotes $1.35 \cdot 10^{14}$. In addition to the characteristics of satellite lines, data for the resonance lines 3C, 3D, and 3E of Ne-like ions are presented in the table. The wavelengths λ_{exp} were experimentally measured in this work, except those denoted by * and +. The wavelengths of the lines 3C and 3D of Ne-like ions denoted by * were measured in Ref. 18 and were used in this work as references. The wavelength of the 3D line of Y from Ref. 16 was also used as a reference (denoted by +). The wavelengths of the 3E lines of Ne-like ions denoted by ** were measured in this work and were not used as references.

	Transition				Y				
Key	Upper level	J_1	Lower level	J_0	λ_{exp}	λ_{theor}	s^{-1}	s^{-1}	s^{-1}
3C	b3d_	1	[KL]	0	5.5274*	5.5262	1.35+14	0	0
b	b3s*3d_	3/2	[KL]3s	1/2	5.537	5.5371	5.21+13	4.42+13	9.30+13
c	b3p_3d_	3/2	[KL]3p	1/2		5.5471	2.86+13	1.01+14	8.73+13
	b3p_3d_	5/2	[KL]3p	3/2		5.5491	6.12+13	2.39+14	2.92+14
	b3p*3d*	3/2	[KL]3p	3/2	5.549	5.5501	1.10+13	2.64+13	3.09+14
	b3p*3d*	1/2	[KL]3p	3/2		5.5504	2.46+13	4.06+13	2.54+14
d	b3d_3d*	3/2	[KL]3d	3/2	5.556	5.5570	2.55+13	4.17+13	2.38+13
f	b3d_3d*	3/2	[KL]3d	5/2		5.5663	1.11+14	4.17+13	1.04+14
	b3d_3d_	3/2	[KL]3d	3/2	5.566	5.5676	1.45+14	5.84+14	2.08+12
	b3p_3d_	1/2	[KL]3p	1/2		5.5681	1.15+14	2.18+13	3.63+13
g	b3p*3p*	1/2	[KL]3s	1/2		5.5705	5.72+13	2.95+13	3.83+13
	b3p*3d_	1/2	[KL]3p	3/2	5.572	5.5707	1.09+14	4.35+14	6.18+13
	b3d_3d*	7/2	[KL]3d	5/2		5.5727	9.15+13	4.41+14	6.06+14
h	b3p*3d_	3/2	[KL]3p	3/2		5.5761	1.12+14	4.17+13	1.19+14
	b3d_3d_	1/2	[KL]3d	3/2	5.576	5.5769	7.09+13	1.89+13	2.98+13
	b3d_3d*	5/2	[KL]3d	5/2		5.5775	1.30+14	1.31+14	2.05+13
i	b3s*3d_	3/2	[KL]3s	1/2	5.580	5.5822	7.64+13	4.33+13	1.07+14
	b3d*3d*	3/2	[KL]3d	3/2		5.5827	8.31+12	5.34+11	1.78+12
j	b3p_3d*	5/2	[KL]3p	3/2		5.5873	1.14+13	1.18+14	6.23+13
	b3p_3d_	3/2	[KL]3p	1/2	5.588	5.5899	8.71+13	7.54+13	1.61+14
	b3p*3d*	5/2	[KL]3p	3/2		5.5915	2.79+13	1.33+13	5.40+13
k	b3p*3d*	5/2	[KL]3p	3/2	5.598	5.6008	2.48+13	3.36+12	1.77+13
	b3d_3d*	5/2	[KL]3d	3/2		5.6020	6.52+12	7.97+13	3.08+13
l	b3d*3d*	7/2	[KL]3d	5/2	5.605	5.6078	1.07+13	1.74+13	5.30+13
m	b3d_3d*	5/2	[KL]3d	5/2		5.6114	1.51+13	7.97+13	7.14+13
	b3p*3d_	3/2	[KL]3p	3/2	5.610	5.6126	9.39+12	4.21+10	1.60+12
	b3d_3d_	5/2	[KL]3d	3/2		5.6135	3.11+13	1.06+14	1.44+14
p	a3p*3d_	3/2	[KL]3p	1/2	5.689	5.6883	2.99+13	3.29+14	1.10+14
3D	a3d*	1	[KL]	0	5.7039⁻	5.7039	1.22+14	0	0
q	a3p*3p*	3/2	[KL]3s	1/2	5.727	5.7274	5.38+13	3.29+13	7.95+13
r	a3p*3d*	5/2	[KL]3p	3/2		5.7334	5.56+12	2.06+14	3.25+13
	a3d*3d*	3/2	[KL]3d	5/2	5.734	5.7336	5.90+13	6.19+13	1.16+14
	a3s*3d*	1/2	[KL]3s	3/2		5.7345	8.34+13	2.22+13	3.51+13
	a3p*3d*	1/2	[KL]3p	3/2		5.7352	1.05+14	1.03+14	1.02+14
s	a3d*3d*	5/2	[KL]3d	3/2		5.7399	4.75+13	4.87+13	6.77+13
	a3p*3d*	3/2	[KL]3p	1/2		5.7401	7.46+12	6.11+12	1.21+13
	a3p*3d*	5/2	[KL]3p	3/2	5.739	5.7408	4.41+13	3.21+11	1.91+12
	a3d_3d*	1/2	[KL]3d	3/2		5.7425	1.29+14	1.35+14	1.30+14
t	a3p*3d_	3/2	[KL]3p	1/2		5.7483	2.08+13	5.50+12	1.73+13
	a3d*3d*	5/2	[KL]3d	5/2	5.749	5.7498	1.09+14	4.87+13	1.55+14
u	a3d*3d*	3/2	[KL]3d	5/2		5.7550	5.59+13	1.26+13	3.89+13
	a3p_3d*	1/2	[KL]3p	1/2		5.7573	9.46+13	1.69+13	2.83+13
	a3p*3d*	3/2	[KL]3p	3/2	5.756	5.7578	6.60+13	4.56+12	1.70+13
	a3s*3d*	3/2	[KL]3s	1/2		5.7581	4.93+13	1.52+14	1.47+14
v	a3p*3d*	3/2	[KL]3p	1/2	5.760	5.7605	2.36+13	9.98+12	2.69+13
	a3d_3d*	5/2	[KL]3d	3/2		5.7619	8.72+13	6.11+14	4.43+14
w	a3d_3d_	3/2	[KL]3d	3/2		5.7657	7.83+13	4.55+10	1.79+11
	a3p*3d*	5/2	[KL]3p	3/2	5.764	5.7658	5.46+13	3.95+13	1.38+14
x	a3d*3d*	7/2	[KL]3d	5/2		5.7673	5.59+13	2.64+14	3.69+14
3E	a3d_	1	[KL]	0	5.770**	5.7723	2.51+11	0	0
	a3p*3p*	3/2	[KL]3s	1/2		5.7701	1.83+13	3.02+13	4.28+13
	a3d_3d*	5/2	[KL]3d	5/2		5.7719	2.36+13	6.11+14	1.20+14
	a3p*3d_	3/2	[KL]3p	1/2		5.7746	2.10+13	6.81+12	2.06+13

TABLE I. (Continued.)

Key	Upper level	J_1	Lower level	J_0	λ_{exp}	λ_{theor}	s^{-1}	s^{-1}	s^{-1}
						Zr			
3C	b3d_	1	[KL]	0	5.2031*	5.2020	1.49+14	0	0
b	b3s*3d_	3/2	[KL]3s	1/2	5.210	5.2109	5.61+13	4.38+13	9.54+13
c	b3p_3d_	3/2	[KL]3p	1/2	5.223	5.2201	2.34+13	6.93+13	6.87+13
	b3p*3d_	5/2	[KL]3p	3/2		5.2232	7.05+13	2.28+14	3.23+14
	b3p*3d*	3/2	[KL]3p	3/2		5.2234	1.15+13	2.37+13	3.08+13
	b3p*3d*	1/2	[KL]3p	3/2		5.2238	2.63+13	3.82+13	2.60+13
d	b3d_3d*	3/2	[KL]3d	3/2	5.229	5.2293	2.41+13	4.10+13	2.06+13
f	b3d_3d*	3/2	[KL]3d	5/2	5.238	5.2387	1.26+14	4.10+13	1.08+14
	b3d_3d_	3/2	[KL]3d	3/2		5.2396	1.61+14	1.13+12	4.08+12
	b3p_3d_	1/2	[KL]3p	1/2		5.2396	1.30+14	2.30+13	3.87+13
g	b3p*3p*	1/2	[KL]3s	1/2	5.243	5.2393	1.47+13	3.06+13	1.97+13
	b3p*3d_	1/2	[KL]3p	3/2		5.2425	1.21+14	4.40+13	6.42+13
	b3d_3d*	7/2	[KL]3d	5/2		5.2441	1.02+14	4.40+14	6.64+14
h	b3p*3d_	3/2	[KL]3p	3/2	5.247	5.2476	1.25+14	3.41+13	1.06+14
	b3d_3d_	1/2	[KL]3d	3/2		5.2476	7.96+13	1.95+13	3.13+13
	b3d_3d*	5/2	[KL]3d	5/2		5.2489	1.42+14	3.46+12	2.02+13
i	b3s*3d_	3/2	[KL]3s	1/2	5.251	5.2526	8.55+13	3.78+13	1.01+14
	b3d*3d*	3/2	[KL]3d	3/2		5.2717	1.27+13	9.88+11	1.68+12
j	b3p_3d*	5/2	[KL]3p	3/2	5.258	—	—	—	—
	b3p_3d_	3/2	[KL]3p	1/2		5.2600	9.55+13	7.20+13	1.64+14
	b3p*3d*	5/2	[KL]3p	3/2		5.2609	3.35+13	1.82+12	1.04+13
k	b3p*3d*	5/2	[KL]3p	3/2	5.268	5.2702	3.32+13	1.27+13	5.50+13
	b3d_3d*	5/2	[KL]3d	3/2		5.2703	6.19+12	7.18+13	2.81+13
l	b3d*3d*	7/2	[KL]3d	5/2	5.278	5.2755	1.22+13	1.78+13	5.78+13
m	b3d_3d*	5/2	[KL]3d	5/2		5.2798	1.68+13	7.18+13	7.64+13
	b3p*3d_	3/2	[KL]3p	3/2		5.2806	1.07+13	2.17+11	7.75+11
	b3d_3d_	5/2	[KL]3d	3/2		5.2814	3.45+13	1.08+14	1.57+14
p	a3p*3d_	3/2	[KL]3p	1/2	5.362	5.3606	2.94+13	3.46+14	1.08+14
3D	a3d*	1	[KL]	0	5.3790*	5.3785	1.41+14	0	0
q	a3p*3p*	3/2	[KL]3s	1/2	5.399	5.3987	5.69+13	4.68+13	1.00+14
r	a3p*3d*	5/2	[KL]3p	3/2	5.406	5.4050	2.91+12	2.12+14	1.72+13
	a3d*3d*	3/2	[KL]3d	5/2		5.4062	7.13+13	6.17+13	1.27+14
	a3s*3d*	1/2	[KL]3s	1/2		5.4058	9.76+13	2.83+13	4.39+13
	a3p*3d*	1/2	[KL]3p	3/2		5.4073	1.23+14	1.05+14	1.21+14
s	a3d*3d*	5/2	[KL]3d	3/2		5.4106	5.01+13	3.97+13	5.42+13
	a3p*3d*	3/2	[KL]3p	1/2		5.4084	6.83+12	5.70+12	1.08+13
	a3p*3d*	5/2	[KL]3p	3/2	5.413	5.4126	5.89+13	3.82+13	2.15+13
	a3d_3d*	1/2	[KL]3d	3/2		5.4135	1.61+14	1.00+14	1.22+14
t	a3p*3d_	3/2	[KL]3p	1/2		5.4167	2.27+13	5.97+12	1.88+13
	a3d*3d*	5/2	[KL]3d	5/2	5.421	5.4206	1.31+14	3.97+13	1.41+14
u	a3d*3d*	3/2	[KL]3d	5/2		5.4256	6.21+13	1.20+13	3.78+13
	a3p_3d*	1/2	[KL]3p	1/2		5.4268	1.17+14	1.96+13	3.30+13
	a3p*3d*	3/2	[KL]3p	3/2	5.425	5.4279	7.18+13	4.58+12	1.72+13
	a3s*3d*	3/2	[KL]3s	1/2		5.4260	5.68+13	1.67+14	1.68+14
v	a3p*3d*	3/2	[KL]3p	1/2		5.4276	2.78+13	1.13+13	3.11+13
	a3d_3d*	5/2	[KL]3d	3/2	5.430	5.4313	1.04+14	6.37+14	5.20+14
w	a3d_3d*	3/2	[KL]3d	3/2		5.4349	9.31+13	6.32+10	2.49+11
	a3p*3d*	5/2	[KL]3p	3/2	5.434	5.4355	6.06+13	4.27+13	1.50+14
x	a3d*3d*	7/2	[KL]3d	5/2		5.4370	6.44+13	2.71+14	4.16+14
3E	a3d_	1	[KL]	0	5.442**	5.4426	2.20+11	0	0
	a3p*3p*	3/2	[KL]3s	1/2	5.434	5.4370	2.73+13	1.75+13	3.93+13
	a3d_3d*	5/2	[KL]3d	5/2	5.442	5.4414	2.44+13	6.37+14	1.22+14
	a3p*3d_	3/2	[KL]3p	1/2		5.4409	2.43+13	7.68+12	2.33+13

TABLE I. (*Continued.*)

Key	Transition				Nb				
	Upper level	J_1	Lower level	J_0	λ_{exp}	λ_{theor}	s⁻¹	s⁻¹	s⁻¹
3C	b3d_	1	[KL]	0	4.9057*	4.9047	1.64+14	0	0
b	b3s*3d_	3/2	[KL]3s	1/2	4.911	4.9117	6.00+13	4.31+13	9.71+13
	b3p_3d_	3/2	[KL]3p	1/2		4.9235	3.02+13	1.05+14	9.35+13
	b3p*3d_	5/2	[KL]3p	3/2		4.9243	8.02+13	2.18+14	3.52+14
c	b3p*3d*	3/2	[KL]3p	3/2	4.924	4.9239	1.18+13	2.16+13	3.05+13
	b3p*3d*	1/2	[KL]3p	3/2		4.9243	2.77+13	3.57+13	2.61+13
d	b3d_3d*	3/2	[KL]3d	3/2	4.928	4.9288	2.26+13	4.01+13	1.77+13
	b3d_3d*	3/2	[KL]3d	5/2		4.9383	1.42+14	4.01+13	1.11+14
f	b3d_3d_	3/2	[KL]3d	3/2	4.938	4.9388	1.74+14	1.82+12	6.71+12
	b3p_3d_	1/2	[KL]3p	1/2		4.9386	1.47+14	2.40+13	4.09+13
	b3p*3p*	1/2	[KL]3s	1/2		4.9350	4.31+12	2.76+13	7.46+12
g	b3p*3d_	1/2	[KL]3p	3/2	4.942	4.9416	1.35+14	4.46+13	6.67+13
	b3d_3d*	7/2	[KL]3d	5/2		4.9430	1.14+14	4.39+14	7.23+14
	b3p*3d_	3/2	[KL]3p	3/2		4.9463	1.39+14	2.90+13	9.50+13
h	b3d_3d_	1/2	[KL]3d	3/2	4.946	4.9458	8.93+13	2.02+13	3.29+13
	b3d_3d*	5/2	[KL]3d	5/2		4.9476	1.55+14	3.56+12	2.08+13
i	b3s*3d_	3/2	[KL]3s	1/2	4.950	4.9505	9.58+13	3.25+13	9.34+13
	b3d*3d*	3/2	[KL]3d	3/2		4.9484	2.04+13	3.93+11	1.39+12
	b3p_3d*	5/2	[KL]3p	3/2		—	—	—	—
j	b3p_3d_	3/2	[KL]3p	1/2	4.955	4.9577	1.05+14	6.90+13	1.66+14
	b3p*3d*	5/2	[KL]3p	3/2		4.9577	2.85+13	3.22+13	9.07+13
k	b3p*3d*	5/2	[KL]3p	3/2		4.9680	4.10+13	3.41+13	1.12+14
	b3d_3d*	5/2	[KL]3d	3/2	4.968	4.9664	5.81+12	6.47+13	2.53+13
l	b3d*3d*	7/2	[KL]3d	5/2		4.9710	1.39+13	1.86+13	6.36+13
	b3d_3d*	5/2	[KL]3d	5/2		4.9760	1.86+13	6.47+13	8.09+13
m	b3p*3d_	3/2	[KL]3p	3/2	4.974	4.9766	1.17+13	4.03+12	9.72+12
	b3d_3d_	5/2	[KL]3d	3/2		4.9771	3.82+13	1.10+14	1.70+14
p	a3p*3d_	3/2	[KL]3p	1/2	5.061	5.0602	2.84+13	3.60+14	1.05+14
3D	a3d*	1	[KL]	0	5.0799*	5.0801	1.63+14	0	0
q	a3p*3p*	3/2	[KL]3s	1/2	5.096	5.0972	5.82+13	6.42+13	1.20+14
	a3p*3d*	5/2	[KL]3p	3/2		5.1040	1.12+12	2.15+14	6.70+12
r	a3d*3d*	3/2	[KL]3d	5/2	5.106	5.1061	8.53+13	6.26+13	1.39+14
	n3s*3d*	1/2	[KL]3s	1/2		5.1047	1.13+14	3.34+13	5.15+13
	a3p*3d*	1/2	[KL]3p	3/2		5.1067	1.43+14	1.08+14	1.21+14
	a3d*3d*	5/2	[KL]3d	3/2	5.111	5.1087	5.23+13	3.14+13	4.13+13
s	n3p*3d*	3/2	[KL]3p	1/2	5.106	5.1043	6.14+12	5.20+12	9.33+12
	a3p*3d*	5/2	[KL]3p	3/2	5.111	5.1117	7.48+13	9.54+12	5.08+13
	a3d_3d*	1/2	[KL]3d	3/2		5.1122	1.87+14	8.69+13	1.18+14
t	a3p*3d_	3/2	[KL]3p	1/2		5.1129	2.35+13	6.02+12	1.90+13
	a3d*3d*	5/2	[KL]3d	5/2	5.118	5.1189	1.55+14	3.14+13	1.22+14
	a3d*3d*	3/2	[KL]3d	5/2		5.1236	6.83+13	1.14+13	3.66+13
u	a3p_3d*	1/2	[KL]3p	1/2		5.1240	1.39+14	2.18+13	3.72+13
	a3p*3d*	3/2	[KL]3p	3/2	5.123	5.1256	7.70+13	4.45+12	1.68+13
	a3s*3d*	3/2	[KL]3s	1/2		5.1217	6.42+13	1.74+14	1.86+14
v	a3p*3d*	3/2	[KL]3p	1/2		5.1226	3.21+13	1.25+13	3.50+13
	a3d_3d*	5/2	[KL]3d	3/2	5.127	5.1283	1.23+14	6.61+14	6.05+14
w	a3d_3d*	3/2	[KL]3d	3/2		5.1319	1.10+14	1.11+11	4.37+11
	a3p*3d*	5/2	[KL]3p	3/2	5.131	5.1329	6.66+13	4.54+13	1.62+14
x	a3d*3d*	7/2	[KL]3d	5/2		5.1342	7.38+13	2.78+14	4.67+14
3E	a3d_	1	[KL]	0	5.139**	5.1404	1.81+11	0	0
	a3p*3p*	3/2	[KL]3s	1/2	5.131	5.1319	3.99+13	7.87+12	2.41+13
	a3d_3d*	5/2	[KL]3d	5/2	5.139	5.13858	2.48+13	6.61+14	1.22+14
	a3p*3d_	3/2	[KL]3p	1/2		5.1351	2.73+13	8.42+12	2.57+13

TABLE I. (Continued.)

	Transition				Mo				
Key	Upper level	J_1	Lower level	J_0	λ_{exp}	λ_{theor}	s^{-1}	s^{-1}	s^{-1}
3C	$b3d_-$	1	$\|KL\|$	0	4.6325*	4.6314	1.80+14	0	0
b	$b3s*3d_-$	3/2	$\|KL\|3s$	1/2	4.636	4.6367	6.37+13	4.22+13	9.79+13
c	$b3p_-3d_-$	3/2	$\|KL\|3p$	1/2	4.650	4.6473	2.51+13	8.44+13	7.49+13
	$b3p*3d_-$	5/2	$\|KL\|3p$	3/2		4.6494	9.03+13	2.08+14	3.78+14
	$b3p*3d*$	3/2	$\|KL\|3p$	3/2		4.6484	1.20+13	1.99+13	2.99+13
	$b3p*3d*$	1/2	$\|KL\|3p$	3/2		4.6489	2.88+13	3.31+13	2.59+13
d	$b3d_-3d*$	3/2	$\|KL\|3d$	3/2	4.655	4.6526	2.10+13	3.93+13	1.50+13
f	$b3d_-3d*$	3/2	$\|KL\|3d$	5/2	4.661	4.6622	1.59+14	3.93+13	1.14+14
	$b3d_-3d_-$	3/2	$\|KL\|3d$	3/2		4.6623	1.83+14	2.66+12	9.92+12
	$b3p_-3d_-$	1/2	$\|KL\|3p$	1/2		4.6620	1.64+14	2.50+13	4.30+13
g	$b3p*3p*$	1/2	$\|KL\|3s$	1/2	4.665	4.6553	1.56+12	2.53+13	2.94+12
	$b3p*3d_-$	1/2	$\|KL\|3p$	3/2		4.6651	1.50+14	4.53+13	6.93+13
	$b3d_-3d*$	7/2	$\|KL\|3d$	5/2		4.6662	1.26+14	4.38+14	7.85+14
h	$b3p*3d_-$	3/2	$\|KL\|3p$	3/2	4.670	4.6694	1.53+14	2.54+13	8.64+13
	$b3d_-3d_-$	1/2	$\|KL\|3d$	3/2		4.6685	1.00+14	2.09+13	3.46+13
	$b3d_-3d*$	5/2	$\|KL\|3d$	5/2		4.6708	1.67+14	3.91+12	2.28+13
i	$b3s*3d_-$	3/2	$\|KL\|3s$	1/2	4.673	4.6729	1.07+14	2.74+13	8.36+13
	$b3d*3d*$	3/2	$\|KL\|3d$	3/2		4.6779	3.45+13	2.41+11	8.76+11
j	$b3p_-3d*$	5/2	$\|KL\|3p$	3/2	4.689	4.6911	4.35+13	6.15+13	1.53+14
	$b3p_-3d_-$	3/2	$\|KL\|3p$	1/2	4.678	4.6798	1.15+14	6.62+13	1.67+14
	$b3p*3d*$	5/2	$\|KL\|3p$	3/2		4.6793	3.40+13	2.45+13	8.54+13
k	$b3p*3d*$	5/2	$\|KL\|3p$	3/2		—	—	—	—
	$b3d_-3d*$	5/2	$\|KL\|3d$	3/2		4.6871	5.42+12	5.84+13	2.25+13
l	$b3d_-3d*$	7/2	$\|KL\|3d$	5/2	4.689	4.6913	1.60+13	1.97+13	7.05+13
m	$b3d_-3d*$	5/2	$\|KL\|3d$	5/2	4.695	4.6968	2.04+13	5.84+13	8.48+13
	$b3p*3d_-$	3/2	$\|KL\|3p$	3/2		4.6980	9.71+12	3.74+13	2.20+13
	$b3d_-3d_-$	5/2	$\|KL\|3d$	3/2		4.6975	4.23+13	1.12+13	1.84+14
p	$a3p*3d_-$	3/2	$\|KL\|3p$	1/2	4.783	4.7841	2.67+13	3.68+14	9.86+13
3D	$a3d*$	1	$\|KL\|$	0	4.8052*	4.8059	1.86+14	0	0
q	$a3p*3p*$	3/2	$\|KL\|3s$	1/2	4.819	4.8199	5.73+13	8.53+13	1.35+14
r	$a3p*3d*$	5/2	$\|KL\|3p$	3/2		4.8273	1.93+11	2.17+14	1.16+12
	$a3d*3d*$	3/2	$\|KL\|3d$	5/2		4.8302	1.01+14	6.39+13	1.52+14
	$a3s*3d*$	1/2	$\|KL\|3s$	1/2		4.8280	1.30+14	3.74+13	5.81+13
	$a3p*3d*$	1/2	$\|KL\|3p$	3/2	4.829	4.8304	1.65+14	1.10+14	1.30+14
s	$a3d*3d*$	5/2	$\|KL\|3d$	3/2		4.8313	5.39+13	2.40+13	2.99+13
	$a3p*3d*$	3/2	$\|KL\|3p$	1/2		4.8249	5.45+12	4.73+12	7.90+12
	$a3p*3d*$	5/2	$\|KL\|3p$	3/2	4.835	4.8353	9.15+13	1.61+13	8.22+13
	$a3d_-3d*$	1/2	$\|KL\|3d$	3/2		4.8354	2.12+14	8.10+13	1.17+14
t	$a3p*3d_-$	3/2	$\|KL\|3p$	1/2		4.8336	2.30+13	5.64+12	1.78+13
	$a3d*3d*$	5/2	$\|KL\|3d$	5/2	4.841	4.8416	1.82+14	2.40+13	1.01+14
u	$a3d*3d*$	3/2	$\|KL\|3d$	5/2		4.8461	7.45+13	1.07+13	3.51+13
	$a3p_-3d*$	1/2	$\|KL\|3p$	1/2		4.8458	1.60+14	2.34+13	4.04+13
	$a3p*3d*$	3/2	$\|KL\|3p$	3/2	4.845	4.8479	8.14+13	4.25+12	1.61+13
	$a3s*3d*$	3/2	$\|KL\|3s$	1/2		4.8422	7.04+13	1.74+14	1.99+14
v	$a3p*3d*$	3/2	$\|KL\|3p$	1/2		4.8423	3.61+13	1.36+13	3.85+13
	$a3d_-3d*$	5/2	$\|KL\|3d$	3/2	4.849	4.8500	1.45+14	6.85+14	6.97+14
w	$a3d_-3d*$	3/2	$\|KL\|3d$	3/2		4.8534	1.29+14	1.67+11	6.59+11
	$a3p*3d*$	5/2	$\|KL\|3p$	3/2	4.854	4.8549	7.30+13	4.78+13	1.73+14
x	$a3d*3d*$	7/2	$\|KL\|3d$	5/2		4.8560	8.41+13	2.84+14	5.19+14
3E	$a3d_-$	1	$\|KL\|$	0	4.861**	4.8626	1.36+11	0	0
	$a3p*3p*$	3/2	$\|KL\|3s$	1/2	4.854	4.8516	5.78+13	1.92+12	6.88+12
	$a3d_-3d*$	5/2	$\|KL\|3d$	5/2	4.861	4.8604	2.48+13	6.85+14	1.19+14
	$a3p*3d_-$	3/2	$\|KL\|3p$	1/2	4.854	4.8541	2.95+13	8.94+12	2.74+13

than 1 mÅ in all four cases, so we have in the table $\lambda_{\text{theor}} = \lambda_{\text{exp}}$.

The trident fgh is the most prominent element of the spectrum; it was recorded earlier in the form of a single amorphous spectrum element. The difference between λ_{exp} and λ_{theor} reaches 1.5 mÅ; the experimental "trident," as in the model, has the largest intensity within the satellite structure.

The i peak in the model spectrum is present for Y and Zr ions. For Nb and Mo ions, it merges with the fgh trident, but for Nb ion the right part of the profile is distinct enough nevertheless, and λ can be measured. The experimental spectra correspond to the model predictions.

The j peak, like the c peak, is well separated. Their intensities are close to each other in the model calculations as well as in the experimental spectra.

A very strange situation occurs for the peaks k, l, and m. The experimental spectra have bright lines located near the suggested peaks k and m, but their wavelengths sometimes differ from the theoretical ones by 3 mÅ (there is no such significant deviation for other peaks), and their intensities for yttrium differ from the theoretical ones more than by a factor of two. For the three remaining elements, the intensities do not differ so strongly, but the l peak is indiscernible in the experimental spectrum.

The p peak is reliably recorded for all the four elements. This is the first of the satellite lines considered whose upper level contains a hole $\overline{2p_{3/2}}$ (see Table I). The experimental and theoretical wavelengths of the p peak and all remaining peaks of this group (from q to w) coincide with the same accuracy, 1 mÅ, as for the satellites considered with a hole in $\overline{2p_{3/2}}$.

The peaks q, r, s, t, u, v, and w (merged with x) exhibit good agreement between λ_{theor} and λ_{exp}. For almost all the peaks, the wavelength difference does not even reach 1 mÅ. The intensities of this group of lines correspond better to the model calculations as well. For the niobium ion, the model shape of the t and u peaks depends strongly on the excitation regime (see Fig. 3). This special feature is reflected in the experimental spectrum: the spectrum integrated over time and space has a resulting envelope with no dip between the peaks t and u.

The peaks w and x were not recorded separately for any of the elements in view of the integrated nature of the spectra. But the width of the total experimental profile in yttrium probably reflects the superposition of two shifted profiles.

For the peaks y and z, possible prototypes in the experimental spectrum can be suggested, but the large number of extraneous lines in this spectral range precludes any definitive conclusions. For this reason, only peaks for yttrium ions are shown in Figs. 3 and 4. The wavelengths λ_{theor} of these peaks and λ_{exp} of the assumed prototypes differ no more than by 2 mÅ. Two more spikes are seen to the right of the z peak in both model and experimental spectra. Their wavelengths also correspond to the theoretical calculations within acceptable limits. However, the experimental intensities of the spikes y, z, and the subsequent ones exceed those predicted theoretically by too much to

consider the identification to be conclusive. These spikes are not indicated in the figures for the remaining three elements, although the situation here is analogous to that illustrated by the example of yttrium.

The identification of the 3E ($2p^6\,^1S_0$–$2p^53d\,^3P_1$) lines for all four elements may be considered an important result of this work. As seen from the experimental spectra of Fig. 4, the 3E line is well isolated. In our work (Ref. 13), the selenium 3E line was blended by a very intense x satellite. In this case, a satellite profile is apparently contained within the 3E line for all four elements, from yttrium to molybdenum. But the intensity of this satellite is low, according to the calculations. The wavelengths of the 3E lines coincide with the calculated one to better than 2 mÅ.

In summary, note that the distinctions between the experimental and theoretical values of the wavelengths do not exceed 2 mÅ for any of the lines investigated (except k,l,m). Most often, it is only 1 mÅ, and we have systematically $\lambda_{\text{exp}} \leqslant \lambda_{\text{theor}}$.

5. DEPENDENCE OF SATELLITE LINE RELATIVE INTENSITY ON PLASMA PARAMETERS

Satellites of multiply charged ion resonance lines are known to be reliable "thermometers." The satellite intensity normalized to the intensity of the corresponding resonance line varies substantially with temperature, and depends weakly on density. It should be remembered, however, that the intensities of the resonance lines themselves are not described by coronal approximation formulas, and the intensity ratio of the satellite and the resonance line is naturally dependent on N_e. Moreover, the recombination channel of populating the upper levels of the resonance lines from the states of fluorine-like ions cannot be forgotten either, because the temperature of plasma with a significant fraction of Ne- and Na-like ions cannot be very high. On the whole, the problem of measuring T_e using the satellite lines of Na-like ions is quite analogous to that of measuring T_e using satellites and resonance lines of K-spectra. At present, a detailed estimate of autoionization level excitation rate is needed for a reliable application of this method.

Assuming all the assumptions made in the process of constructing the model spectrum to be valid, we have a trivial dependence (1) of the intensity I on the electron density N_e. It is important to emphasize that relation (1) itself expresses a typical feature of dielectron satellites: the number of dielectron recombination events per unit time and unit volume is proportional to the electron density (in contrast to three-particle recombination, which is proportional to N_e^2 and plays a dominant role in populating the excited states at high densities). It is this fact, resulting in identical dependencies of both items in (1) on N_e, that makes it possible to think of satellites as promising spectral lines from the standpoint of plasma charge composition diagnostics.

In our case, of particular importance is the fact that the model spectra obtained for the alternative limiting cases of populating only from a Ne-like ion and only from a Na-like ion have comparable intensities (see Fig. 3) at
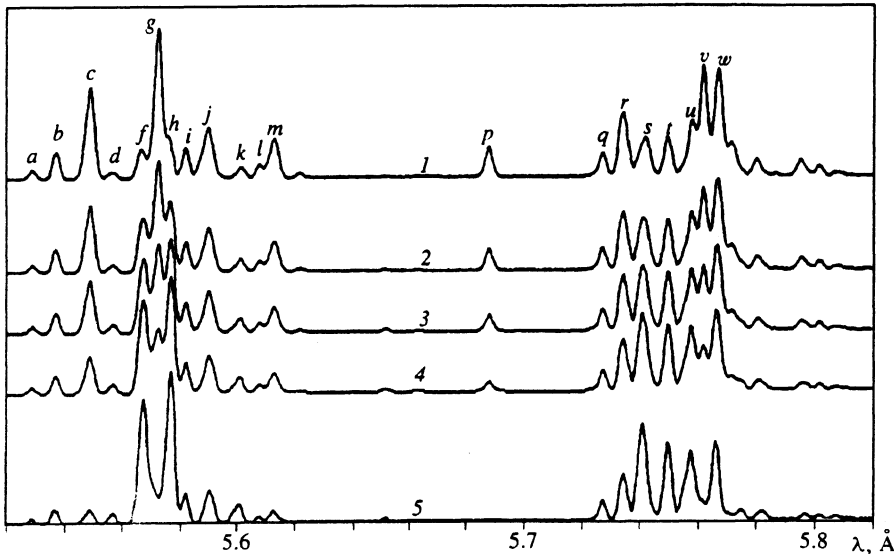
FIG. 5. Envelopes of the satellite structure of the 3C,3D,3e resonance lines (the lines themselves are not presented) of Y XXX ion at $T_e=900$ eV and different ratios f of Ne-like and Na-like ion concentrations:

temperatures typical of plasma sources in which ions of these multiplicities are formed. Such close intensities in combination with radical distinctions of the shapes of limiting envelopes mean that we have an extremely convenient and reliable method for determining the concentration ratio of Ne- and Na-like ions.

Examples of theoretical envelopes of the satellite structure at a temperature $T_e=z^2$ [eV] and different values of $f=N(\text{Ne})/N(\text{Na})$ are given in Fig. 5. Typical features of the envelope appearance changing drastically in structure with the parameter $N(\text{Ne})/N(\text{Na})$ (particularly for the fgh and uvw groups) allow one to hope that the sensitivity of this method for measuring relative concentrations will be high. Naturally, the utilization of potential advantages of this method for studying space–time evolution of the ionization is possible only if spectral resolution is adequate. If the spectrum of the structure is not resolved or is blended with the lines of other ions, one should use the relative intensities of isolated satellites, for instance the c, p, and s lines.

Let us examine the dependence of the relative intensities on T_e and f. Using expression (1), we can write the ratio of the intensities of two satellite lines I_1 and I_2 in the form

$$\varkappa_{12}=\frac{I_1}{I_2}=\frac{D_1 f+E_1}{D_2 f+E_2},$$

where D_i and E_i are the components of the total intensity resulting from dielectron capture from a Ne-ion and excitation from a Na-like ion, respectively. Selecting a version of a satellite pair with opposite dominant population mechanisms ($D_1 \gg E_1$ but $D_2 \ll E_2$), we have

$$\varkappa_{12}=\frac{D_1}{E_2} f,$$

i.e. the most direct measurement of the concentration ratio f becomes possible. Unfortunately, the ratio D_1/E_1 inevitably depends on temperature in this case because the energy of electron impact excitation considerably exceeds the energy of dielectron capture. However, the presence of sev-

eral independent intensity ratios makes it possible in principle to reconstruct information on physical parameters of plasma in an arbitrary nonstationary ionization state.

6. CONCLUSION

Thus, we have thus demonstrated in the present paper, using several elements from yttrium to molybdenum as an example, that intense structures recorded regularly in the spectra of various plasma sources near the resonance lines of Ne-like ions [i.e., 3C ($^1S_0-2s^22p^53d\ ^1P_1$) and 3D ($^1S_0-2s^22p^53d\ ^3D_1$)] are formed by a combination of dielectron satellite lines resulting from transitions in Na-like ions. For the four ions studied, the experimental spectra within these satellite structures do not require additional assumptions on the presence of intense lines of ions belonging to other isoelectronic sequences for their interpretation. All intense isolated elements of the experimental spectra are satisfactorily described by theoretical model envelopes. In the spectral range investigated, the long-wave length of the resonance lines 3C and 3D, containing several well defined spikes, and the spectral regions lying to the right of the 3E lines and probably including the lines of Mg- and Al-like ions are not yet described. Moreover, the identification of the least intense satellites k, l, and m cannot be considered conclusive, although there are no obvious objections to the identification proposed. The remaining satellite peaks studied may be thought of as reliably identified.

Stating the fact that identification of satellite spectra of Na-like ions in the vicinity of Ne-like ions is performed for the first time in this work, we may conclude that the theoretical calculations for the corresponding ionic structures are reliable. The maximum disagreement between the theoretical and the experimental wavelengths is essentially always less than 2 mÅ, and for the overwhelming majority of the lines studied this disagreement does not exceed 1 mÅ.

The measurement of wavelengths of the satellite lines to high accuracy, good agreement between the model and the experimental spectra, and high sensitivity of the spectrum structure to the plasma parameter variations testify

that the utilization of radiation spectrum of Na-like ions for the high-temperature plasma diagnostics is promising.

[1] V. A. Boiko, A. V. Vinogradov, S. A. Pikuz et al., *X-Ray Spectroscopy of Laser-Produced Plasmas* [in Russian], ser. Radiotekhnika, vol. 27, Moscow (1980).

[2] R. C. Elton, *X-Ray Lasers*, Academic Press, San Diego (1980).

[3] J. Nilsen, J. L. Porter, B. J. MacGowar et al., J. Phys. B: At. Mol. Opt. Phys. **26**, 1243 (1993).

[4] J. Nilsen, P. Beirsdorfer, S. R. Elliott, and A. L. Osterheld, Physica Scripta **47**, 42 (1993).

[5] W. H. Goldstein, B. L. Whitten, A. U. Hazi, and M. H. Chen, Phys. Rev. A **36**, 3607 (1987).

[6] E. V. Aglitskii, V. A. Boiko, O. N. Krokhin et al., Kvant. Elektron. **1**, 2067 (1974).

[7] V. A. Boiko, A. Ya. Faenov, and S. A. Pikuz, J. Quant. Spectrosc. Radiat. Transfer **19**, 11 (1978).

[8] P. G. Burkhalter and D. J. Nagel, Phys. Rev. A **11**, 782 (1975).

[9] H. Gordon, M. G. Hobby, and N. J. Peacock, J. Phys. B **13**, 1985 (1980).

[10] J. F. Seely, T. W. Phillips, R. S. Walling et al. Phys. Rev. A **34**, 2942 (1986).

[11] W. H. Goldstein, R. S. Walling, J. Bailey et al., Phys. Rev. Lett. **58**, 2300 (1987).

[12] O. Peyrusse, P. Combis, M. Louis–Jacquet et al., J. Appl. Phys. **65**, 3802 (1989).

[13] J. Nilsen, S. A. Pikuz, I. Yu. Skobelev et al., Izmer Tekh. No. 5, 3 (1994).

[14] J. Nilsen, S. A. Pikuz, I. Yu. Skobelev et al., Kvant. Elektron. **20**, 1164 12 (1993) [Quantum Electronics **23**, 1010 (1993).

[15] B. A. Bryunetkin, V. M. Dyakin, J. Nilsen et al., Kvant. Elektron. **21**, 142 (1994) [Quantum Electronics **24**, 133 (1994).

[16] J. Nilsen, At. Data and Nucl. Data Tables **41**, 131 (1989).

[17] V. A. Boiko, V. G. Pal'chikov, I. Yu. Skobelev, and A. Ya. Faenov, *X-Ray Spectroscopy of Multiply Charged Ions* [in Russian], Energoatomizdat, Moscow (1988).

[18] E. V. Aglitskii, E. P. Ivanova, S. A. Panin et al., Physica Scripta **40**, 601 (1989).

Translated by A. M. Mozharovskii